PAPER

A lattice Boltzmann–cellular automaton study on dendrite growth with melt convection in solidification of ternary alloys*

A lattice Boltzmann–cellular automaton study on dendrite growth with melt convection in solidification of ternary alloys*

Dong-Ke Sun(孙东科)[1,2,†], Zhen-Hua Chai(柴振华)[3], Qian Li(李谦)[4], and Guang Lin(林光)[5]

[1] School of Mechanical Engineering, Southeast University, Nanjing 211189, China
[2] Open Project of State Key Laboratory of Advanced Special Steel, Shanghai University, Shanghai 200444, China
[3] School of Mathematics and Statistics, Huazhong University of Science and Technology, Wuhan 430074, China
[4] School of Materials Science and Engineering & Materials Genome Institute, Shanghai University, Shanghai 200444, China
[5] Department of Mathematics, School of Mechanical Engineering, Purdue University, West Lafayette, IN 47907, USA

(Received 8 March 2018; revised manuscript received 9 May 2018; published online 10 July 2018)

A lattice Boltzmann (LB)–cellular automaton (CA) model is employed to study the dendrite growth of Al-4.0 wt%Cu–1.0 wt%Mg alloy. The effects of melt convection, solute diffusion, interface curvature, and preferred growth orientation are incorporated into the coupled model by coupling the LB–CA model and the CALPHAD-based phase equilibrium solver, PanEngine. The dendrite growth with single and multiple initial seeds was numerically studied under the conditions of pure diffusion and melt convection. Effects of initial seed number and melt convection strength were characterized by new-defined solidification and concentration entropies. The numerical result shows that the growth behavior of dendrites, the final microstructure, and the micro-segregation are significantly influenced by melt convection during solidification of the ternary alloys. The proposed solidification and concentration entropies are useful characteristics bridging the solidification behavior and the microstructure evolution of alloys.

Keywords: lattice Boltzmann, dendritic growth, numerical simulation, melt convection

PACS: 81.30.Fb, 47.11.–j, 68.08.De, 81.10.–h **DOI:** 10.1088/1674-1056/27/8/088105

1. Introduction

Melt convection is known as an unavoidable phenomenon in solidification of metals and alloys. It directly influences heat and mass transfer during solidification and substantially affects microstructure evolution including dendrite growth, solute segregation, and morphological selection. Dendritic morphology is the most commonly observed in solidification, and it is closely associated with the final properties of metals and alloys. Therefore, modeling of dendrite growth is a fundamental problem to reveal the underlying mechanism of microstructure evolution in solidification. Since most industrial metallic materials are multi-component systems, it is more essential to developing numerical models of dendrite growth for ternary alloys than that for pure metals and binary alloys. Numerical studies on dendrite growth of ternary alloys, especially that in the condition of melt convection, are in great demand nowadays.

In the last few decades, the lattice Boltzmann (LB) method has been rapidly emerging as a powerful and indispensable method for modeling complex systems with fluid flows.[1–5] For the numerical efficiency and parallel computational capability of the LB method, massive notable LB models were developed, and pioneers in computational materials science attempted to model dendrite growth in solidification of pure metals and alloys.[6] The phase-field method is one of the most widely used numerical methods to study the dendrite growth in two- and three-dimensional systems.[7,8] Miller and co-workers[9–12] firstly proposed a single relaxation time (SRT)-based LB-phase field (PF) model to study the anisotropic liquid–solid phase transition and the free dendrite growth of pure metals with moderate buoyancy convection and shear flows. Subsequently, Medvedev and Kassner[11,12] combined the PF and LB models to simulate dendrite growth with liquid flows from a supercooled melt. The PF model was utilized to describe the liquid–solid phase, while the SRT–LB model was accounting for melt convection during dendrite growth. Selzer *et al.*[13] used the PF–LB coupled model and studied the effect of melt convection on dendrite growth during solidification of an Ni–Cu alloy. In these PF–LB coupled models, the PF method was adopted to describe the liquid–solid phase transition, while the LB method was employed to describe the melt convection, heat, and mass transfer during solidification.

The usage of the SRT–LB equation in these models decreases the computational cost in simulations of melt convection and heat/mass transport, but solving the PF equation was computationally expensive, which limited the promotion of the numerical efficiency of the coupled models. Several numerical models integrating the LB method and other techniques were therefore proposed for the simulation of dendrite

*Project supported by the National Natural Science Foundation of China (Grant Nos. 51728601 and 51771118).
†Corresponding author. E-mail: dksun@seu.edu.cn

growth with melt convection. Chakraborty and Chatterjee[14] developed an enthalpy-based hybrid LB model to simulate the liquid–solid phase transition and convection-diffusion phenomena. They stated that the hybrid model was fitting into a thermodynamically consistent manner for non-isothermal systems. Sun *et al.* proposed an LB–CA coupled model to study the dendrite growth with melt convection including forced melt flows and natural convection driven by buoyancy.[15,16] In the LB–CA model, the SRT–LB scheme was used to describe solute diffusion and melt convection, while the CA rule was used to model the liquid–solid phase transition. Their results demonstrated the LB–CA coupled model is numerically stable and computationally efficient with good quantitative capability. After that, Felicelli *et al.* extended the LB–CA coupled models to study dendrite growth in three-dimensional space.[17,18] Jelinek *et al.* developed a large-scale parallel LB–CA model incorporating solute diffusion, heat transfer, melt convection, and phase change.[19] The model was then used to numerically study the two-dimensional dendrite growth with forced convection. In their simulation, the LB method showed very good scalability.

The above studies on dendrite growth by coupling the PF, enthalpy-based, CA models, and the LB method have proved that the LB method is an efficient numerical tool to reveal the correlation between melt flows, heat transfer, and phase transition in solidification. They provide significantly improved computational efficiency in the simulation of dendrite growth of metals and alloys. However, all these studies were focused on the growth of pure crystals and binary alloys. Very few works were devoted to simulating dendrite growth with melt convection in solidification of ternary alloys. Therefore, numerical studies are in great demand for dendrite growth with melt convection in solidification of ternary alloys. Historically, the LB method is originated from the lattice gas automaton which is an advanced CA technique. It is therefore natural to combine the CA and LB models to simulate dendrite growth with and without melt convection.

Recently, a multi-relaxation-time (MRT) LB model was developed to study the three-dimensional dendrite growth and bubble formation in solidification of alloys.[20] It provides an evidence that the MRT–LB-based technique was an alternative solution with good numerical stability to study the dendrite growth of alloys. However, the MRT–LB model is more computationally expensive than the SRT–LB model, and the convective effect of melt on dendrite growth has not been studied in that work. As the melt convection is unavoidable during solidification of alloys, it is of great importance to have a deep understanding of dendrite growth with melt convection.

In the present work, we are aiming to study the dendrite growth of ternary alloys and analyzing the convective effect on microstructure evolution during solidification. We attempt to explain the influencing mechanism of several conditions on morphological evolution by defining the solidification and solute concentration entropies. Considering the CA models are usually more computationally efficient than the PF models, we combine the CA and the LB techniques into a convenient and efficient scheme. The PanEngine, a CALPHAD-based multiphase equilibrium solver, has been used to compute the phase equilibrium in solidification. The melt convection is described by the SRT–LB model for the model's computational efficiency. A scheme fitting into the CA framework is utilized to track the advancement of the liquid/solid interface and describe the evolution of dendrite morphology. In this work, the LB–CA coupled model is extended to study the solidification of the Al-4.0 wt%Cu–1.0 wt%Mg alloy. The effects of initial seed number and convection strength are subsequently investigated in a systematic way. The influencing mechanism of melt convection on micro-segregation is explored by comparing the microstructure evolution, concentration distribution, and solidification entropies during dendrite growth in the conditions of pure diffusion and melt convection. Finally, a summary closes this paper and gives an outlook for future works.

2. Mathematical modeling

2.1. Modeling of convective diffusion

In this work, the SRT–LB method[21,22] is applied to describe melt convection for its numerical efficiency in modeling complex fluid flows. The general formula of the SRT–LB equations with discrete velocities $\boldsymbol{e}_\alpha$ on a D-dimensional lattice can be expressed as

$$\begin{aligned} & f_\alpha(\boldsymbol{x}+\boldsymbol{e}_\alpha\Delta t, t+\Delta t) - f_\alpha(\boldsymbol{x},t) \\ = & -\frac{1}{\tau}\left[f_\alpha(\boldsymbol{x},t) - f_\alpha^{\mathrm{eq}}(\boldsymbol{x},t)\right] + F_\alpha, \end{aligned} \tag{1}$$

where $f_\alpha(\boldsymbol{x},t)$ is the particle distribution function (PDF). It represents the probability of finding a pseudo particle in the α-th direction on the discrete lattice at position $\boldsymbol{x}$ and time t, $\boldsymbol{e}_\alpha$ is the discrete particle velocity, Δt is the time step, τ is the relaxation time, and $f_\alpha^{\mathrm{eq}}(\boldsymbol{x},t)$ is the equilibrium PDF. The last term of the equation is the forcing term as a result of the internal interaction or external fields, which reflects the alteration of PDF caused by the body force $\boldsymbol{F}$ on fluids.

Considering the numerical stability and computational accuracy, we adopt a very commonly used D2Q9 model with the following discrete velocities $\boldsymbol{e}_\alpha$,

$$[\boldsymbol{e}_\alpha, \alpha = 0, ..., 8] = \begin{bmatrix} 0 & c & 0 & -c & 0 & c & -c & -c & c \\ 0 & 0 & c & 0 & -c & c & c & -c & -c \end{bmatrix}, \tag{2}$$

where the lattice speed $c \equiv \Delta x/\Delta t$. Subsequently, the lattice sound speed is $c_{\mathrm{s}} = c/\sqrt{3}$. For the D2Q9 model of the LB

method, the weight coefficient w_α is given as[22]

$$w_\alpha = \begin{cases} 4/9, & \alpha = 0, \\ 1/9, & \alpha = 1,2,3,4, \\ 1/36, & \alpha = 5,6,7,8. \end{cases} \tag{3}$$

The equilibrium PDF can be expressed as

$$f_\alpha^{\rm eq} = w_i \rho \left[1 + \frac{\boldsymbol{e}_\alpha \cdot \boldsymbol{u}}{c_{\rm s}^2} + \frac{(\boldsymbol{e}_\alpha \cdot \boldsymbol{u})^2}{2c_{\rm s}^4} - \frac{\boldsymbol{u}^2}{2c_{\rm s}^2} \right], \tag{4}$$

and the forcing term in Eq. (1) can be computed by[23]

$$F_\alpha = \left(1 - \frac{1}{2\tau}\right) w_i \rho \left[\frac{\boldsymbol{e}_\alpha - \boldsymbol{u}}{c_{\rm s}^2} + \frac{\boldsymbol{e}_\alpha \cdot \boldsymbol{u}}{c_{\rm s}^4} \boldsymbol{e} \right] \cdot \boldsymbol{F} \Delta t. \tag{5}$$

The macroscopic variables such as density ρ, and velocity $\boldsymbol{u}$ in Eqs. (4) and (5) can be calculated from the relevant PDF, respectively:

$$\rho = \sum_{\alpha=0}^{8} f_\alpha, \quad \boldsymbol{u} = \sum_{\alpha=0}^{8} f_\alpha \boldsymbol{e}_\alpha / \rho + \boldsymbol{F} \Delta t. \tag{6}$$

The relaxation times τ is correlated with the kinematic viscosity ν according to the Chapman–Enskog analysis.[24] We have

$$\nu = \left(\tau - \frac{1}{2}\right) c_{\rm s}^2 \Delta t. \tag{7}$$

The convective–diffusion model[25] with PDF $g_\alpha(\boldsymbol{x},t)$ is used for the solute transfer in melt. The governing equation is

$$\begin{aligned} & {g_\alpha}^\sigma (\boldsymbol{x} + \boldsymbol{e}_\alpha \Delta t, t + \Delta t) - {g_\alpha}^\sigma (\boldsymbol{x}, t) \\ = & -\frac{1}{\tau_D^\sigma} \left[g_\alpha^\sigma (\boldsymbol{x}, t) - g_\alpha^{\sigma,{\rm eq}} (\boldsymbol{x}, t) \right] + S_\alpha^\sigma (\boldsymbol{x}, t), \end{aligned} \tag{8}$$

where $g_\alpha^{\sigma,{\rm eq}}(\boldsymbol{x},t)$ represents the equilibrium PDF at $(\boldsymbol{x},t)$, and τ_D^σ is the relaxation times for solute transport. The source term $S_\alpha^\sigma(\boldsymbol{x},t)$ denotes the contribution on concentration of rejected solute during dendrite growth. The macroscopic solute concentration in liquid, $C_{\rm l}^\sigma$, can be calculated from $C_{\rm l}^\sigma = \sum_\alpha g_\alpha^\sigma$. The solute diffusivity in liquid D_l^σ is related to the relaxation times τ and τ_D^σ by the Chapman–Enskog analysis[25] via

$$D_l^\sigma = \frac{1}{3}\left(\tau_D^\sigma - \frac{1}{2}\right) c^2 \Delta t. \tag{9}$$

As there is no melt convection in a solid, the solute transfer in solids is driven only by diffusion. Therefore, the governing equation for solute transport in a solid is

$$\frac{\partial C_{\rm s}^\sigma}{\partial t} = \nabla \cdot (D_{\rm s}^\sigma \nabla C_{\rm s}^\sigma), \tag{10}$$

where $D_{\rm s}^\sigma$ is the diffusion coefficient of the σ-component in a solid.

2.2. Modeling of dendrite growth

Through the SRT–LB model for melt convection and solute transport, we can obtain the local solute concentration in liquid during dendrite growth. According to the concentration, we can obtain the local equilibrium liquidus temperature and compositions at the solid/liquid interface by the CALPHAD-based solver PanEngine.[26] The growth kinetics of dendrites can be described by the difference between the equilibrium liquidus temperature and the local actual temperature at the solid/liquid interface. The modified CA rule[27] is used to model the increment of solid during dendrite growth. In the model, the increment of solid phase at each interface cell is computed by

$$\Delta f_{\rm s}(\boldsymbol{x},t) = \mu_k G_{\rm CA} \Delta T(\boldsymbol{x},t)/c, \tag{11}$$

where $\Delta f_{\rm s}(\boldsymbol{x},t)$ represents the solid phase increment in position $\boldsymbol{x}$ at time t, μ_k is the interface kinetic coefficient, $G_{\rm CA}$ is the geometrical factor depending on the state of the current cell and its neighbors, and $\Delta T(\boldsymbol{x},t)$ denotes the total undercooling. In the simulation, the source terms in Eq. (8) can be calculated via $S_\alpha^\sigma(\boldsymbol{x},t) = w_\alpha \Delta f_{\rm s}(\boldsymbol{x},t)(C_l^{\sigma,*} - C_s^{\sigma,*})$ with the solid fraction increment $\Delta f_{\rm s}(\boldsymbol{x},t)$. Here, $C_l^{\sigma,*}$ and $C_s^{\sigma,*}$ represent the liquid and solid concentrations of the σ-th solute at the interface, respectively. Through solving the convective–diffusion equations, we can obtain the σ-th solute concentrations C_l^σ and C_s^σ. Subsequently, the $C_l^{\sigma,*}$, $C_s^{\sigma,*}$ and the interface equilibrium temperature T^* can be computed by the CALPHAD-based solver, PanEngine.

As the modified CA rule with $G_{\rm CA}$ is simple and efficient, we used the CA scheme to describe the growth kinetics in the present work. In the modified CA scheme, the geometrical factor is defined as

$$G_{\rm CA} = \min\left(1, b_0 \sum_{\alpha=1}^{8} [w_{\alpha,{\rm CA}} s(\boldsymbol{x} + \boldsymbol{e}_\alpha \Delta t)]\right), \tag{12}$$

where b_0 is an empirical coefficient and chosen as $b_0 = 2/5$. For the cubic lattice used in this work, the weight coefficient $w_{\alpha,{\rm CA}}$ is given as suggested in reference[27]

$$w_{\alpha,{\rm CA}} = \begin{cases} 1, & \alpha = 1,2,3,4, \\ 1/\sqrt{2}, & \alpha = 5,6,7,8. \end{cases} \tag{13}$$

The $s(\boldsymbol{x} + \boldsymbol{e}_\alpha \Delta t)$ is an indicator function that equals 1 on a solid node and 0 on a liquid node. The mathematical expression of $G_{\rm CA}$ is very simple, but it reflects the geometrical relation between growing velocity and lattice spaces. The influence on the growth of a node from the nearest neighbors is stronger than that from the next-nearest neighbors. The effects of interface curvature and preferred orientations are incorporated into the model by defining the total undercooling

$$\Delta T = \Delta T_{\rm t} + \Delta T_{\rm c} + \Delta T_{\rm r}, \tag{14}$$

and the Gibbs–Thomson relationship

$$\Delta T_{\mathrm{r}} = -\gamma_{\mathrm{a}} K(1 - 15\varepsilon_1 \cos[4(\theta - \theta_p)]), \tag{15}$$

where ΔT_{t}, ΔT_{c}, and ΔT_{r} are undercoolings accounting for the thermal, solutal, and curvature effects, respectively. γ_{a} is the average Gibbs–Thomson coefficient, K is the local curvature of the liquid/solid interface, ε_1 is the anisotropic degree of the interfacial energy, θ is the angle between the normal vector of the solid/liquid interface and the horizontal direction, and θ_{p} is the preferred orientation of dendrite growth. The anisotropies of interfacial kinetics and thermodynamics are both considered in the present model as that suggested in Ref. [27]. The interfacial kinetic coefficient μ_{k} in Eq. (11) is assumed as

$$\mu_{\mathrm{k}} = \mu_{k,0}(1 + \varepsilon_2 \cos[4(\theta - \theta_{\mathrm{p}})]), \tag{16}$$

where $\mu_{k,0}$ is the kinetic coefficient without considering the interfacial anisotropy, and ε_2 is the anisotropic degree of interfacial kinetics. The local interface curvature, K and the growth preferred angle θ can be calculated from[28]

$$K = -\frac{(\partial_x f_{\mathrm{s}})^2 \partial_y^2 f_{\mathrm{s}} - 2\partial_x f_{\mathrm{s}} \partial_y f_{\mathrm{s}} \partial_{xy}^2 f_{\mathrm{s}} + (\partial_y f_{\mathrm{s}})^2 \partial_x^2 f_{\mathrm{s}}}{[(\partial_x f_{\mathrm{s}})^2 + (\partial_y f_{\mathrm{s}})^2]^{3/2}}, \tag{17}$$

$$\theta = \arctan(\partial_y f_{\mathrm{s}} / \partial_x f_{\mathrm{s}}). \tag{18}$$

Since the thermal diffusivity of alloys is about several orders of magnitude larger than the solutal diffusivity, the temperature field in the domain is considered to be uniform with a given artificial thermal undercooling ΔT_{t}. Under the dilute solution assumption, the solutal undercooling can be computed on the local liquid concentration C_{l}^{σ} by $\Delta T_{\mathrm{c}} = \sum_{\sigma} m_{\mathrm{l}}^{\sigma}(C_{\mathrm{l}}^{\sigma} - C_0^{\sigma})$. Here, C_0^{σ} is the initial concentration and m_{l}^{σ} is the liquidus slope of the σ-th solute, respectively. In the present work, we used the PanEngine to obtain the solutal undercooling via $\Delta T_{\mathrm{c}} = T^* - T_{\mathrm{loc}}$, where T_{loc} represents the local temperature.

2.3. Definition of solidification entropy

In order to quantitatively describe multiple dendrite growths, the solidification entropy is defined as

$$S_{\mathrm{s}} = -\sum_{p=1}^{n} p(a_{\mathrm{p}}) \log p(a_{\mathrm{p}}), \tag{19}$$

where $p(a_{\mathrm{p}})$ is the function symbolizing probabilities of finding the state a_{p}, and n is the total number of states in the solidification system. For the present problem, there are three states, i.e., liquid, solid, and interface. Suppose the computational domain is divided into $M_i \times M_j$ cells. The cell in the discrete space can be marked as (i, j). Once the cell (i, j) is full of solid phase, we have $a_S = 1$, $a_L = 0$, and $a_I = 0$. Then, the $p(a_{\mathrm{S}})$ can be computed through $p(a_{\mathrm{S}}) = \sum_{i,j} a_{\mathrm{S}}(i, j)/(M_i M_j)$. After determining $p(a_{\mathrm{S}})$, $p(a_{\mathrm{L}})$, and $p(a_{\mathrm{I}})$, the S_{s} can be computed according to Eq. (19). It should be announced that the S_{s} is inspired by the Shannon entropy of an n-state system.[29] Physically, the S_{s} indicates the disorder degree of a solidification system, and the value of S_{s} depends on the complexity of phases in the system. The S_{s} can be used to compare the disorder degree of a given system under various conditions. Similarly, the concentration entropy can be defined as

$$S_{\mathrm{c}} = -\sum_{q=1}^{m} p(a_q) \log p(a_q), \tag{20}$$

where $p(a_q)$ represents the probabilities of finding the concentration state a_q, and m is the total number of concentration states a_q of the system. Suppose the concentration range $[C_{\min}, C_{\max}]$ is divided into n segments with interval ΔC. The state a_{c} includes concentrations $C \in [C_{\min}, C_{\min} + q\Delta C]$. In the present work, we set $m = 50$ for all the simulations and then quantitatively compared the simulated phase and concentration fields by S_{s} and S_{c}.

The Al–Cu–Mg alloys are commonly used in academical and industrial experiments. Therefore, we take the Al-4.0 wt%Cu–1.0 wt%Mg ternary alloy as a typical object of ternary alloys in the present work. We considered a square domain of 500 μm×500 μm filled with the undercooled melt. Initially, seven seeds were randomly placed in the domain. The melt temperature in the domain was assumed to be uniform initially, and cooled down from the liquidus temperature at a constant cooling rate of R_{c}. For the case of melt convection, the melt was supposed to be the incompressible Newtonian fluid driven by a body force $\boldsymbol{F}$. The body force can evoke an acceleration $\boldsymbol{a}$. By varying the $\boldsymbol{a}$, we can obtain different flow fields with various streaming strength. The four sides of the domain were considered as the periodic boundary condition for the flow and concentration fields. The solidified dendrite was set to be rigid and stationary, and the solid/liquid interface was set as the non-slip boundary condition. In the LB model, the bounce-back rule was used to deal with the boundary condition. The physical parameters used in this work are listed in Table 1.

Table 1. Parameters used in this work.[27,30–33]

Parameters	Dimension	Value
$D_{\mathrm{l,Cu}}$	$\mathrm{m/s^2}$	$1.05 \times 10^{-7} \exp(-2856/T)$
$D_{\mathrm{s,Cu}}$	$\mathrm{m/s^2}$	$2.90 \times 10^{-5} \exp(-15600/T)$
$D_{\mathrm{l,Mg}}$	$\mathrm{m/s^2}$	$9.90 \times 10^{-5} \exp(-8610/T)$
$D_{\mathrm{s,Mg}}$	$\mathrm{m/s^2}$	$3.70 \times 10^{-5} \exp(-14854/T)$
δ_{k}	1	3.0×10^{-1}
ε	1	2.0×10^{-2}
γ_a	mK	1.7×10^{-7}
$\mu_{\mathrm{k},0}$	m/sK	3.0×10^{-4}

3. Results and discussion

3.1. Single dendrite growth

To study the convective effect on growth, we firstly simulated the single dendrite growth with and without melt convection as described in the methods. A periodic boundary condition was imposed on the domain sides for solute fields in the present simulations. For the dendrite growth with melt convection, an acceleration of $\boldsymbol{a} = (0, 0.01)$ m/s^2 was exerted on the melt. Initially, a crystal seed was placed in the center of the square domain. The seed started to grow up driven by the initial thermal undercooling, $\Delta T_{t,0}$. Figure 1 displays the comparison of the morphological evolution of dendrites in the conditions of pure diffusion and melt convection. As shown in Figs. 1(a)–1(d), the seed grew into four-fold symmetrical dendrite without melt convection, and the solute field demonstrated symmetrical characteristic under the same condition. In Fig. 1, C represents the concentration of solute Cu. In the condition of melt convection, the primary dendritic arms grew up at the same growing rate. Both the simulated dendrite and solute field were symmetric with respect to the x and y-axis. However, the four-fold symmetrical feature of the single dendrite was broken when melt convection was induced in the solidification domain. As shown in Figs. 1(e)–1(h), the melt convection was developed with the growth of dendrite, the melt flowed from the bottom side to the top side of the domain, and the primary dendritic arms grew up with different speed. It can also be found that the primary dendritic arm in the upstream region is a bit longer than that downstream. That is because the solute was flushed away from the upstream to the downstream. As the liquidus slope around the present alloy composition is negative, the higher the solute concentration, the lower the solute undercooling. Higher solute concentration in the downstream region results in lower solute undercoolings. It subsequently leads to a lower growing rate of the downstream arm. While the solute concentration of liquid close to the horizontal arms is lowest contrary to those near the arms parallel to the flowing direction. The horizontal arms grew faster than the others. The dendrite and solute field only displays a symmetrical feature with respect to the y-axis. Therefore, melt convection can alter the dendrite pattern during solidification.

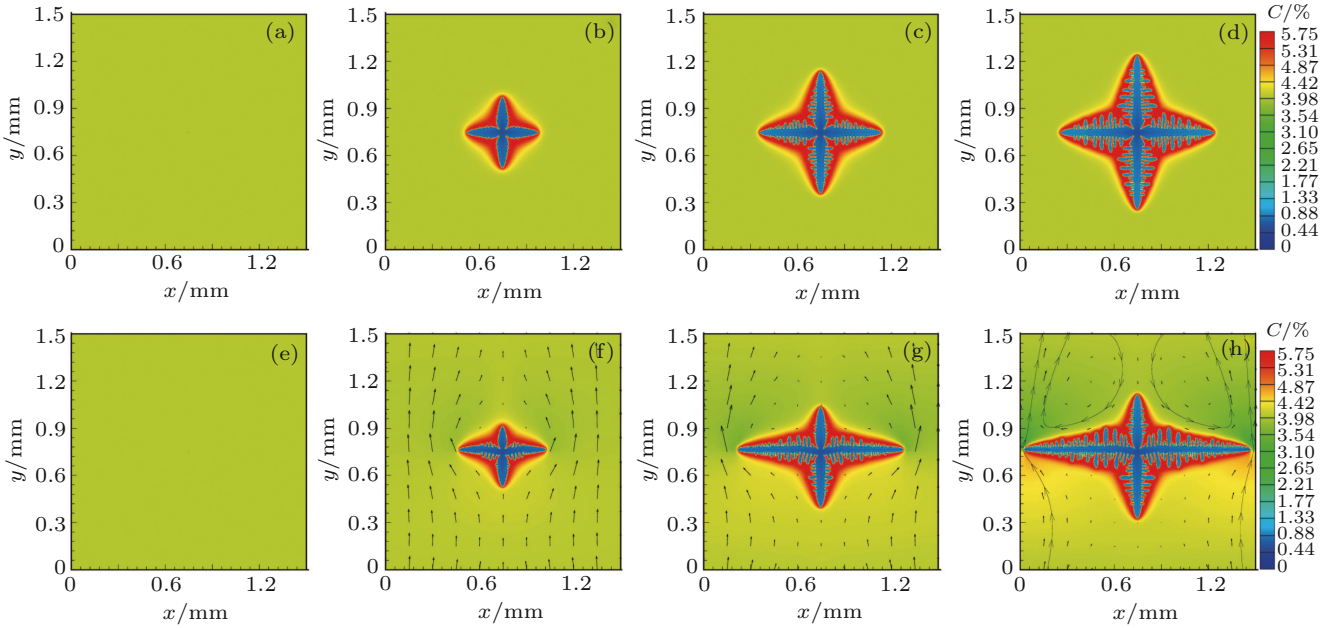

Fig. 1. (color online) Morphologies of single dendrite growth [(a)–(d)] in pure diffusion condition and [(e)–(h)] in the presence of melt convection at $\boldsymbol{a} = (0, 0.01)$ m/s^2: (a) and (e) initial state: (b) and (f) $F_s = 2.0\%$; (c) and (g) $F_s = 5.0\%$; (d) and (h) $F_s = 8.0\%$.

Figure 2 shows the characteristics of the simulated dendrite growth in Fig. 1. As displayed in Fig. 2(a), the dendrite grew at a relatively low rate at the initial solidification stage for both the conditions of pure diffusion and melt convection. After the initial solidification stage, the growing rate became faster and faster (1.5 s $< t <$ 2.5 s), and the dendrite entered into a quickly developed stage (2.5 s $< t <$ 3.5 s). Then, the dendrite grew at another relatively low rate, and the solidification went into its final solidification stage. It can be found that the melt convection advanced the fast developing stage of the dendrite, but it did not change the tendency of dendrite growth. Figure 2(b) depicts solidification entropy S_s as a function of solid fraction F_s. It can be seen that the melt convection slightly affects the solidification entropy. The S_s for the dendrite under melt convection is a little lower than that without melt convection. As the S_s is defined to characterize the disorder degree of a multiphases system, we can conclude that the melt convection plays a less important role in affecting the dendrite morphology under the present condition.

However, the melt convection can influence the solute

fields significantly rather than the dendrite morphology. As shown in Figs. 2(c) and 2(d), the profiles of concentration entropy against solid fraction for melt convection display undulance at the initial slowly growing and the fast developing stages of dendrites, while the profiles for pure diffusion are smoother at the same stages. It is interesting that the melt convection changed the solute fields, broke the symmetric morphology but hardly affected the disorder degree of the solidification system. A possible reason is that the solidification only occurs at the solid/liquid (S/L) interface but the melt streams strongly in the liquid region away from the S/L interface. The further from the S/L interface, the stronger of the melt convection. The flow velocity close to the S/L interface approximates to zero. The solute concentration in the liquid far from the S/L interface can be directly affected by melt convection, while the solute concentration at the S/L interface is indirectly influenced by the convection. Because the solidification only occurs at the S/L interface, the disorder of the system was less changed by liquid flows. Therefore, the profiles of S_c^1–F_s and S_c^2–F_s for the single dendrite growth with melt convection are significantly different from that without melt convection, while the profiles of S_s–F_s are almost the same as each other under both conditions.

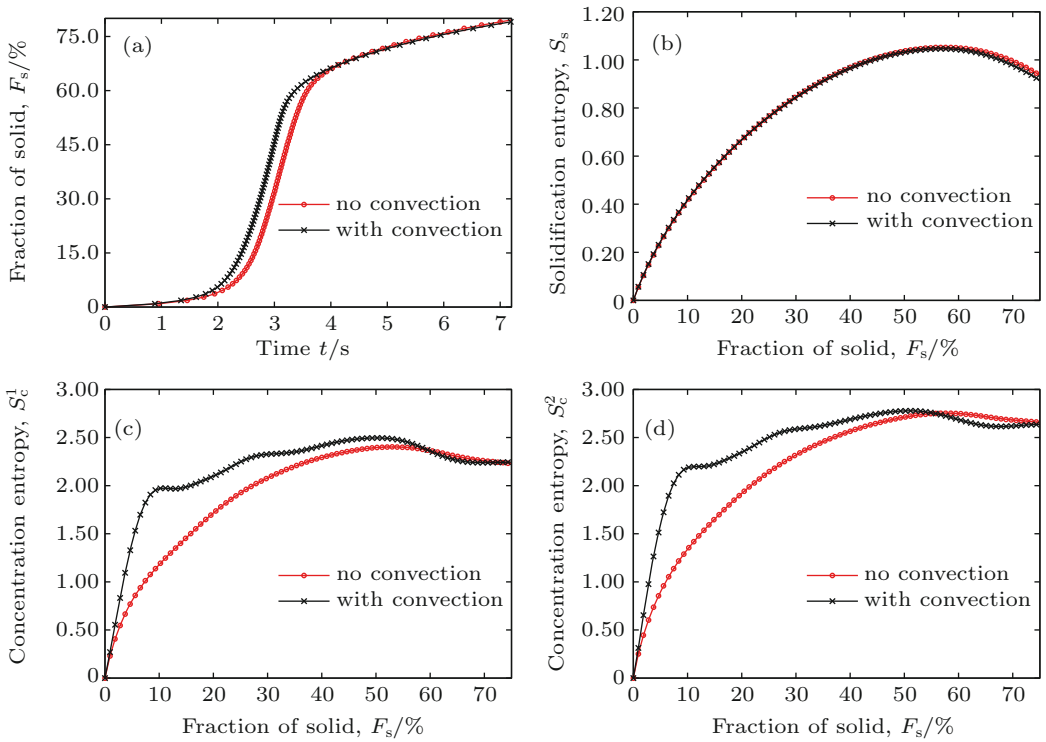

Fig. 2. (color online) Characteristics of single dendrite growth under $R_c = 5.0$ K/s in the conditions of pure diffusion and melt convection at $\boldsymbol{a} = (0, 0.01)$ m/s^2: (a) Time history of the solid fraction, and (b) solidification entropy S_s, (c) concentration entropy of solute Cu, and (d) concentration entropy of solute Mg as functions of solid fraction F_s.

3.2. Multiple dendrite growth

To study the convective effect on the growth of multiple dendrites, we randomly placed 20 seeds into the computational domain. Both the conditions of pure diffusion and melt convection were studied in the present simulations. Other conditions were set the same as those in Fig. 1. Figure 3 shows the morphological evolution of multiple dendrites without and with melt convection. Figure 4 shows the profiles of characteristics for the multiple dendrite growth. Initially, the seeds freely grew up and the solutes were rejected from the S/L interface into the liquid. The solute concentrations around the S/L interface rose with the development of dendrites, as shown in Figs. 3(a), 3(b), 3(e), and 3(f). As the liquid–solid phase transition only occurs at the interface and the interface area is small at the initial stage, the dendrites grew relatively slowly at the initial slowly growing stage ($t < 0.5$ s), as shown in Fig. 4(a). The solutes were then transferred from the region near the S/L interface into the liquid farther away from the interface. As the interface area expanded, the dendrites grew faster and faster (0.5 s $< t <$ 1.5 s). When the dendrites entered the relatively fast developing stage (1.5 s $< t <$ 2.5 s), the primary dendritic arms became longer and stronger, and the secondary dendritic arms started to generate with the growth of dendrites, as shown in Figs. 3(c) and 3(g). After this stage, the primary and secondary dendritic arms continued to grow at a relatively low rate, and the solute concentration became very high in the inter-dendrite region, as shown in Figs. 3(d) and 3(h). Through the whole process of the multiple dendrite growth without melt convection, the solute was transferred

only by diffusion, as shown in Figs. 3(a)–3(d). For the melt convection, the solute atoms were transferred by both diffusion and convection, as shown in Figs. 3(e)–3(h). When the dendrites grew into a closed domain, the melt convection was blocked by the solid phase. Despite the fact that the acceleration was still imposed on the liquid, the melt convection became weaker and weaker with the solidification. As shown in Figs. 3(g)–3(h), the arrows representing melt convection direction and strength vanished. Therefore, the melt convection can hardly affect the dendrite growth at this period.

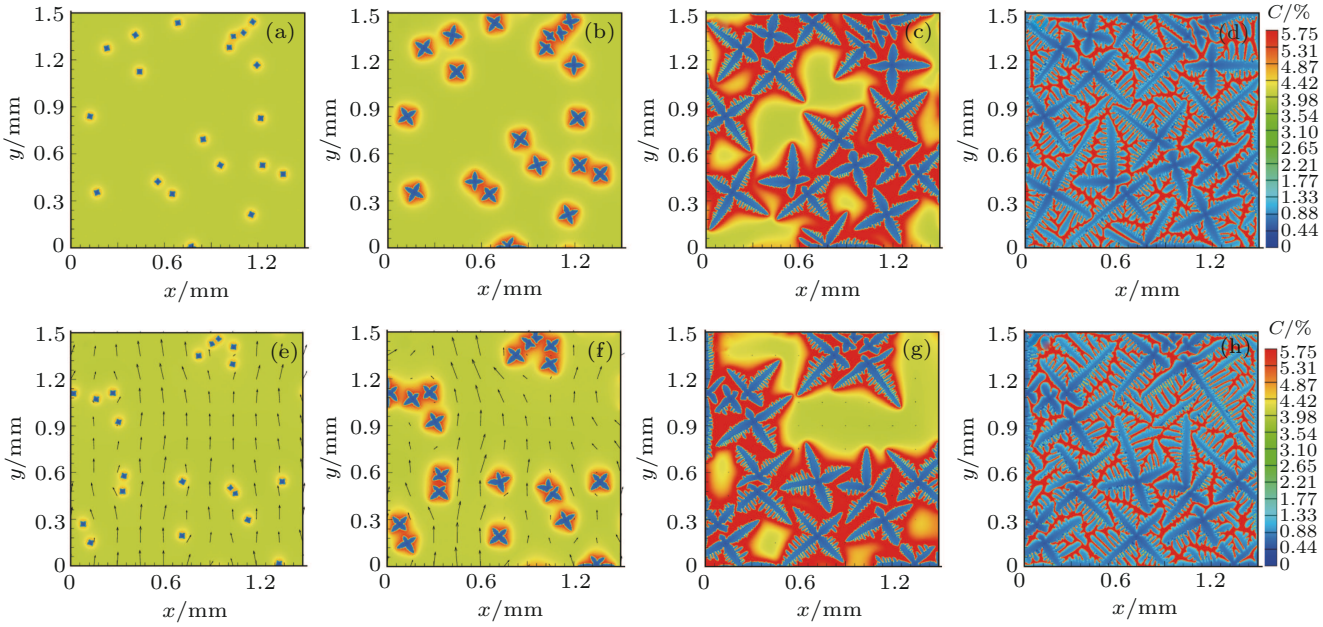

Fig. 3. (color online) Morphologies of multiple dendrite growth [(a)–(d)] without and [(e)–(h)] with melt convection at $\boldsymbol{a} = (0, 0.01)$ m/s^2: (a) and (e) $F_s = 1.0\%$; (b) and (f) $F_s = 5.0\%$; (c) and (g) $F_s = 30.0\%$; and (d) and (h) $F_s = 75.0\%$.

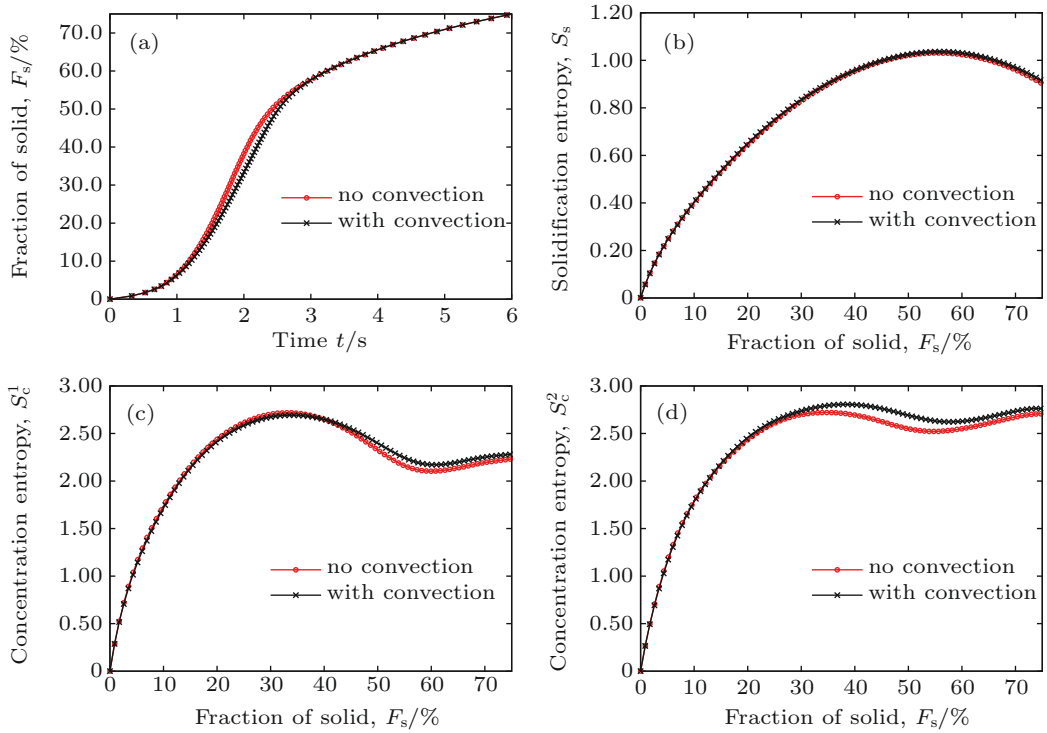

Fig. 4. (color online) Characteristics of multiple dendrite growth without and with melt convection of $\boldsymbol{a} = (0, 0.01)$ m/s^2 at $R_c = 5.0$ K/s: (a) time history of the solid fraction, and (b) solidification entropy S_s, (c) concentration entropy of solute Cu, (d) concentration entropy of solute Mg as functions of solid fraction F_s.

Figure 4 suggests that the characteristics of dendrites and solute field were changed by the melt convection. As shown in Fig. 4(a), the time history of solid fraction displays the same increasing trends for both the conditions of pure diffusion and melt convection. The whole process of multiple dendrite growth can be divided into three stages, namely

the initial slowly growing stage, the relatively fast developing stage, and the final slowly solidifying stage at the lower growth rate. The same trends can be found in Fig. 2(a). However, it seems that the melt convection inhibited the dendrite growth at 1.5 s $< t <$ 2.5 s in Fig. 4(a), while the melt convection promoted the dendrite growth at 1.5 s $< t <$ 2.5 s in Fig. 2(a). The reason is that the seeds were randomly placed in the domain and the randomicity resulted in such retardation of dendrite growth under the condition of melt convection. Through the whole process of multiple dendrite growth, the solidification and concentration entropies demonstrate the same increasing and decreasing trends under both the conditions of pure diffusion and melt convection. At the final stage, the solidification and concentration entropies for the dendrite growth with melt convection are higher than the entropies for the dendrite growth without convection, which implies that the melt convection increased the disorder degrees of phases and solute concentrations.

3.3. Effect of initial seed number

The grain refinement technique is usually used to enhance the mechanical properties of alloys. By using the grain refinement technique, we can get various numbers of initial seeds during the solidification of alloys. To analyze the effect of initial seed number on dendrite morphological evolution, we carried out simulations of the solidification of Al-4.0 wt%Cu–1.0 wt%Mg alloy in the presence of melt convection. Figure 5 shows the simulated morphologies of multiple dendrite growths at $R_c = 5.0$ K/s and $\boldsymbol{a} = (0, 0.02)$ m/s^2 with the initial seed numbers of 20, 40, 60, and 80, respectively. It can be seen that the seeds formed into the dendrite pattern with their preferred orientations. The primary dendritic arms grew into long and thick shapes, while secondary dendritic arms were short and thin perpendicular to their affiliated primary arms. With the increase of the initial seed number, the primary dendritic arms became shorter and shorter, and the secondary dendritic arms appeared less and less. To make a quantitative comparison, we also used the solid fraction, solidification entropy, and solute concentration entropy as characteristics for the present multiple dendrite growths. Figure 6 shows the profiles of characteristics of the multiple dendrite growths platted in Fig. 5. The history of F_s shows the same regularities at various initial seed numbers, as depicted in Fig. 6(a). However, the increase of the initial seed number accelerates the appearance of the fast developing stage of solidification. The reason is that there is a competition between phase change domination and diffusion domination in solidification. The interface area is enlarged with the increase of initial seed number. The liquid–solid phase transition occurs rapidly with the larger interface area. Therefore, the increase of initial seed number can raise the dendrite growth rate. Figures 6(b)–6(d) display that the solidification and solute concentration entropies have the same going up and down trends versus solid fraction despite different initial seed numbers. With the increase of solid fraction, the solidification entropies initially rise up rapidly, and then reach their peak values around $F_s = 55.0\%$. After the peaks, the solidification entropies start to decrease. However, varying the initial seed number can change the solidification and solute concentration entropies. The larger the seed number, the lower the entropies. That is because the dendrites were competing for growing space during solidification. Given a solidification domain, more seeds implies less space for dendrites to grow into. The rejected solute atoms get less space to diffuse in the condition of a larger initial seed number. Subsequently, the solute concentrations are getting higher in the inter-dendrite region. The primary and secondary arms are thus inhibited from developing. Therefore, the increase of initial seed number can decrease the disorder degree of the multiphase and multicomponent system.

3.4. Effect of convection strength

The convection strength is a key factor influencing the growing process of dendrites. To make a quantitative study, we carried out simulations of multiple dendrite growth with the acceleration magnitude in the range $|\boldsymbol{a}| \in [0.00, 0.08]$ m/s^2 with an interval of 0.01 m/s^2. Initially, 20 seeds were placed in the domain full of undercooling liquid. Other conditions were set to be the same as those in Fig. 3. The averaged solidification rate was measured by summarizing the rate $\mathrm{d}F_s/\mathrm{d}t$ with the increase of solid fraction via $R_s = \sum_{F_s=1\%}^{75\%}(\mathrm{d}F_s/\mathrm{d}t)/75$. The solidification and solute concentration entropies were measured when $F_s = 75.0\%$ for all the simulations. Figure 7 shows the characteristics of multiple dendrite growth as functions of the acceleration magnitude $|\boldsymbol{a}|$. The scattered dots depict the actual data while the solid lines show the smoothed data series. As shown in Figs. 7(a) and 7(b), both the solidification rate and the solidification entropy decrease with the acceleration increase, which implies that strengthening melt convection would inhibit the solidification process and decrease the disorder degree of the multiphase system. It seems that the present simulations overturn the conventional understanding of the convective effect on dendrite growth. In the conventional understanding, melt convection promotes dendrite growth and thus the solidification rate will be promoted with the acceleration increase. However, the acceleration increase retarded the solidification processes in the present simulations. The possible reason is that the melt convection promotes den-

drite growth at the initial slow-solidifying stage. The dendritic arms in the condition of larger accelerations would grow rapidly with the mediation of convection. The convection promotes the dendrite growth at this stage. When the dendrites become longer, stronger, and approaching each other, the convection will be blocked. As the present simulation is carried out in two-dimensional space, and the dendrite is supposed to be fixed in the domain, therefore, three-dimensional numerical simulations are required to examine the promotion of dendrite arms by melt flows in future. After the initial stage, the convection becomes weaker and weaker, it can hardly affect the dendrite growth. As the solute field was changed at the initial stage, the dendrites keep growing in the influenced solute fields after the initial stage. Figures 7(c) and 7(d) show that the solute concentration entropies appear with increasing trends and then show decreasing trends when raising the flow field. The solidification and concentration entropies are synchronously changed with the strengthening of melt convection. It suggests that the melt convection changed the solute distributions in liquid and subsequently affected the solute segregation during dendrite growth. Generally, the solute transfer driven by convection is stronger than that driven by diffusion. Therefore, in a lower strength flow field, i.e., at a smaller $|\boldsymbol{a}|$, the melt convection can accelerate the rejected solute atoms to transfer from the liquid region near the S/L interface to the liquid region far from the S/L interface. While in a higher strength flow field, i.e., at a larger $|\boldsymbol{a}|$, the melt convection promotes dendrite growth, and primary dendritic arms can grow more rapidly than in a lower strength flow field. The developed arms block melt convection in the solidification domain and subsequently decrease the solute transfer. There exists a competition between the convective effect on growth and the block effect on convection. It is the competition that dominates the trends of the entropies against the flow field strength.

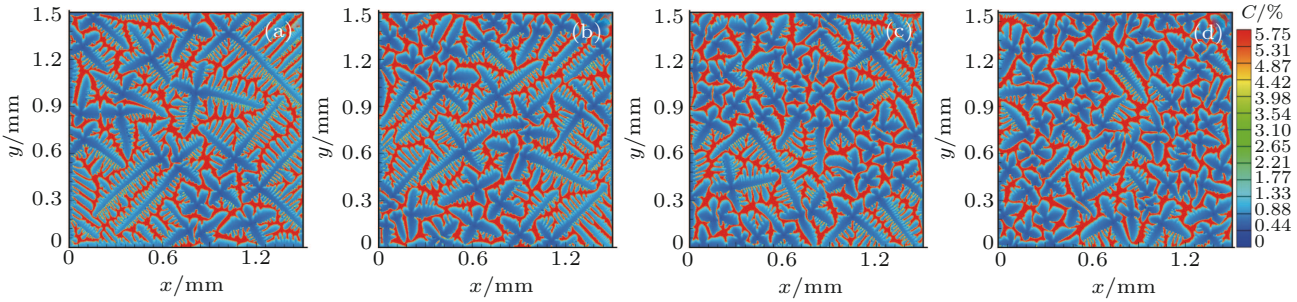

Fig. 5. (color online) Morphologies of multiple dendrite growth in the presence of melt convection at $R_c = 5$ K/s and $\boldsymbol{a} = (0, 0.02)$ m/s^2: (a) 20 seeds, $F_s = 75.0\%$, (b) 40 seeds, $F_s = 75.0\%$, (c) 60 seeds, $F_s = 75.0\%$, and (d) 80 seeds, $F_s = 75.0\%$.

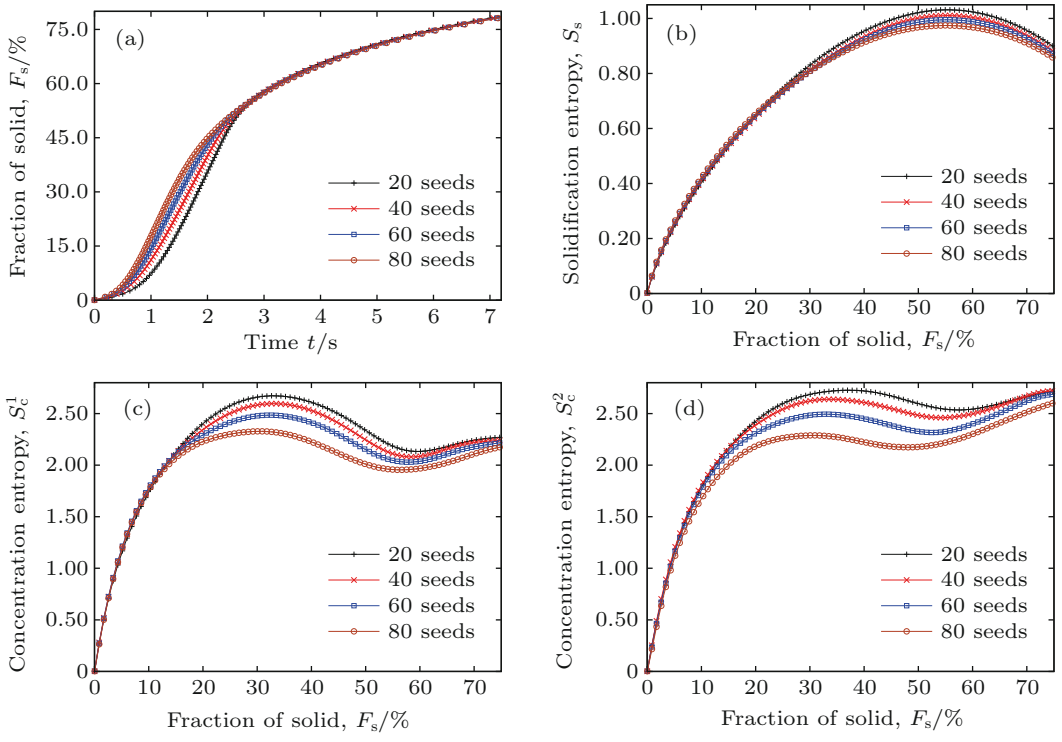

Fig. 6. (color online) Characteristics of multiple dendrite growth in the presence of melt convection of $\boldsymbol{a} = (0, 0.02)$ m/s^2 at $R_c = 5.0$ K/s and initial seed numbers of 20, 40, 60, 80: (a) time history of the solid fraction, and (b) solidification entropy S_s, (c) concentration entropy of solute Cu, (d) concentration entropy of solute Mg as functions of solid fraction F_s.

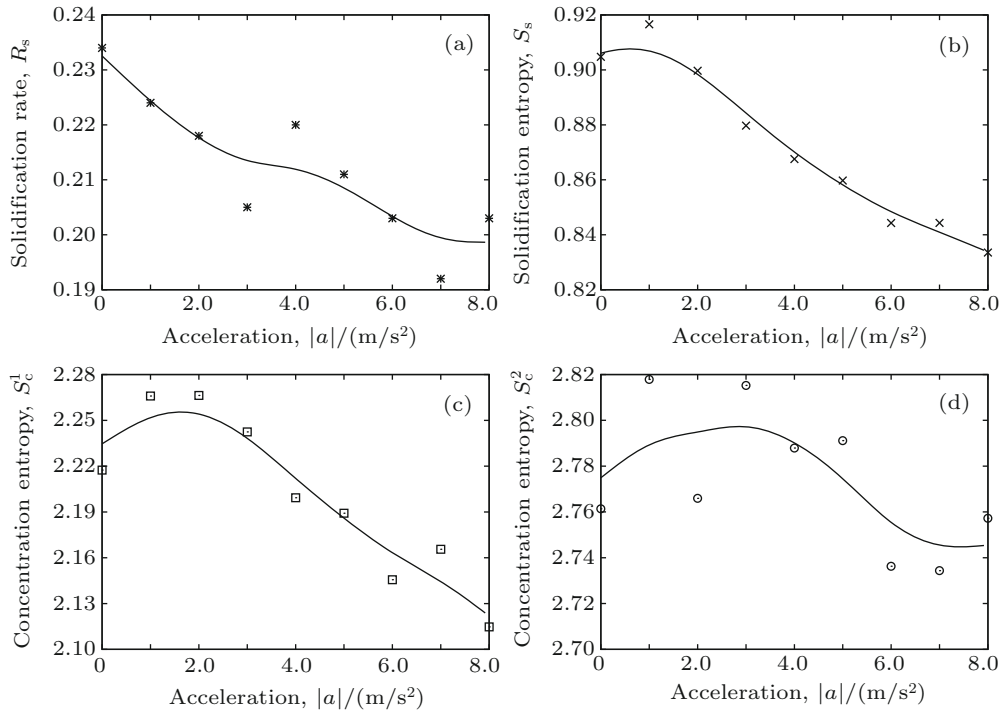

Fig. 7. Characteristics of multiple dendrite growth in the presence of melt convection at $|\boldsymbol{a}| \in [0.00, 0.08]$ m/s^2 with an interval of 0.01 m/s^2: (a) time history of the solid fraction, and (b) solidification entropy S_s, (c) concentration entropy of solute Cu, and (d) concentration entropy of solute Mg as functions of acceleration magnitude $|\boldsymbol{a}|$.

4. Conclusion

The LB–CA coupled model was used to study dendrite growth of ternary alloys in the presence of melt convection. The CA rule is utilized to describe the advancement of the liquid/solid interface, coupling with the SRT–LB equations for the melt convection and the solute transport in solidification. The solidification and concentration entropies were defined to describe dendritic morphologies and solute distributions. The present study shows that the entropies can quantitatively characterize the complexities of ternary solidification systems. Simulations of dendrite growth were carried out in the conditions of pure diffusion and melt convection under various initial seed numbers and convection strengths. The melt convection obviously changes the solute fields and breaks the morphological symmetry at the initial stage of solidification. The increase of initial seed number can inhibit the generation of dendritic arms and decrease the disorder degree of phases and components in the solidification system. With the increase of seed numbers, the melt convection plays a less and less important role in affecting dendrite growth. The developed dendritic arms can evoke a block effect on melt convection, and subsequently decrease solute transfer in solidification. The competition between convective and block effects leads to solute distribution changes with the increase of convective strength.

The present work provides a potential solution to the prediction for dendritic morphology and solute distribution in the solidification of ternary alloys. The present model allows numerical studies of solidification features like solute micro-segregation, grain-refinement, and precipitation of solid phases. It would be extended to perform further investigations for three dimensional dendrite growth of multi-component alloys.

Acknowledgment

The authors thank Prof. Mingfang Zhu at Southeast University (China) and Dr. Hui Xing at Northwestern Polytechnical University (China) for their helpful discussion.

References

[1] Chen L, Kang Q, Robinson B A, He Y L and Tao W Q 2013 *Phys. Rev. E* **87** 043306
[2] Zhang C B, Deng Z L and Chen Y P 2014 *Int. J. Heat Mass Transfer* **70** 322
[3] Gan Y B, Xu A G, Zhang G C and Succi S 2015 *Soft Matter* **11** 5336
[4] Chen Y P, Wu L Y and Zhang L 2015 *Int. J. Heat Mass Transfer* **82** 42
[5] Liang H, Li Q X, Shi B C and Chai Z H 2016 *Phys. Rev. E* **93** 033113
[6] Eshraghi M, Jelinek B and Felicelli S 2015 *JOM* **67** 1786
[7] Xing H, Zhang L, Song K, Chen H and Jin K 2017 *Int. J. Heat Mass Transfer* **104** 607
[8] Xing H, Ankit K, Dong X, Chen H and Jin K 2018 *Int. J. Heat Mass Transfer* **117** 1107
[9] Miller W, Succi S and Manutti D 2001 *Phys. Rev. Lett.* **86** 3578
[10] Miller W, Rasin I and Pimentel F 2004 *J. Cryst. Growth* **266** 283
[11] Medvedev D and Kassner K 2005 *Phys. Rev. E* **72** 056703
[12] Medvedev D, Fischaleck T and Kassner K 2007 *J. Cryst. Growth* **303** 69
[13] Selzer M, Jainta M and Nestler B 2009 *Phys. Status Solidi B* **246** 1197
[14] Chakraborty S and Chatterjee D 2007 *J. Fluid Mech.* **592** 155
[15] Sun D K, Zhu M F, Pan S Y and Raabe D 2009 *Acta Mater.* **57** 1755
[16] Sun D K, Zhu M F, Pan S Y, Yang C R and Raabe D 2011 *Comput. Math. Appl.* **61** 3585
[17] Yin H, Felicelli S D and Wang L 2011 *Acta Mater.* **59** 3124
[18] Eshraghi M, Felicelli S D and Jelinek B 2012 *J. Cryst. Growth* **354** 129

[19] Jelinek B, Eshraghi M, Felicelli S and Peters J F 2014 *Comput. Phys. Commun.* **185** 939
[20] Sun D K, M Zhu M F, Wang J and Sun B D 2016 *Int. J. Heat Mass Transfer* **94** 474
[21] Chen S Y, Chen H D, Martinez D and Matthaeus W H 1991 *Phys. Rev. Lett.* **67** 3776
[22] Qian Y H, d'Humi'eres D and Lallemand P 1992 *Europhys. Lett.* **17** 479
[23] Guo Z L, Zheng C G and Shi B C 2002 *Phys. Rev. E* **65** 046308
[24] Lallemand P and Luo L S 2000 *Phys. Rev. E* **62** 4982
[25] Deng B, Shi B C and Wang G C 2005 *Chin. Phys. Lett.* **22** 267
[26] Chen S L, Daniel S, Zhang F, Chiang Y A, Yan X Y, Xie F Y, Schmid-Fetzer R and Oates W A 2002 *CALPHAD* **26** 175
[27] Zhu M F, Lee S Y and Hong C P 2004 *Phys. Rev. E* **69** 061610
[28] Beltran-Sanchez L and Stefanescu D M 2004 *Metall. Mater. Trans. A* **35** 2471
[29] Shannon C E 1948 *Bell Syst. Tech. J.* **27** 379
[30] Yan X Y, Chen S L, Xie F Y and Chiang Y A 2002 *Acta Mater.* **50** 2199
[31] Jacot A and Rappaz M 2002 *Acta Mater.* **50** 1909
[32] Ode M, Lee J S, Kim S G, Kim W T and Suzuki T 2000 *ISIJ Int.* **40** 870
[33] Zhu M F, Cao W S, Chen S L, Hong C P and Chiang Y A 2007 *J. Phase Equilib. Diff.* **28** 130